Macromolecules

pubs.acs.org/Macromolecules Article

Regulating Dynamics of Polyether-Based Triblock Copolymer Hydrogels by End-Block Hydrophobicity

Hyunjoon Jung,[§] Seong-Eun Gang,[§] Jung-Min Kim, Tae-Young Heo, Sangho Lee, Eeseul Shin, Byeong-Su Kim, and Soo-Hyung Choi*

Cite This: https://dx.doi.org/10.1021/acs.macromol.0c01939 Read Online

ACCESS | Metrics & More | Article Recommendations | Supporting Information

ABSTRACT: The relaxation dynamics of poly(ethyl glycidyl ether-*co*-isopropyl glycidyl ether-*b*-ethylene oxide-*b*-ethyl glycidyl ether-*co*-isopropyl glycidyl ether) triblock copolymer hydrogels were investigated as a function of the end-block hydrophobicity and temperature primarily using the oscillatory rheometer, which is crucial to understand the unique viscoelastic behaviors including injectability and self-healing property of the self-assembled hydrogels. Lower critical solution temperature behavior of the poly(alkyl glycidyl ether) end-blocks was harnessed by random copolymerization of poly(ethyl glycidyl ether) (EGE) and poly(isopropyl glycidyl ether) (iPGE), resulting in the remarkable temperature responsiveness of the hydrogel. As the fraction of hydrophilic monomer (i.e., EGE) increases, the sol-to-gel transition occurs at higher temperature and higher polymer concentration. The hydrogel relaxation measured by the oscillatory rheometer becomes faster with decreasing temperature and increasing fraction of hydrophilic monomers. In particular, we observed that a small increment of the hydrophilic monomer fraction significantly reduces the unfavorable interaction between the end-block and aqueous media, resulting in faster hydrogel relaxation dynamics. All polyether-based hydrogels showed biocompatibility and injectability, indicating promising soft materials for biological and biomedical applications. The results are discussed in terms of the current understanding of self-assembled triblock copolymer hydrogels, and particular attention is paid to the issue of chain dynamics.

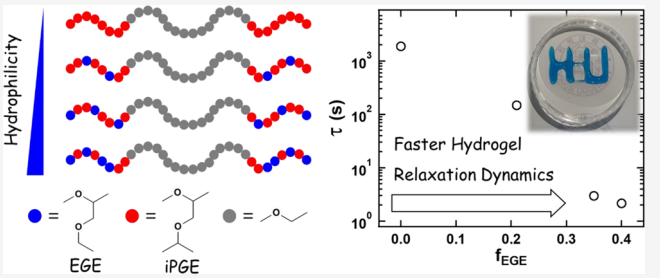

INTRODUCTION

Self-assembly of ABA-type triblock copolymers in midblock selective solvent at sufficiently high polymer concentration produces physically cross-linked and percolated gel, where the end-blocks form micellar cores that are bridged by midblocks.[1−6] In aqueous solvent, poly(ethylene oxide) (PEO) has been comprehensively used as a midblock owing to its biocompatibility, low toxicity, and temperature responsiveness.[7−11] Furthermore, the suitable design of the end-blocks endows stimuli-responsiveness to temperature,[12−16] pH,[12,17,18] ionic strength,[14,19,20] and mechanical force,[21−23] resulting in the unique rheological and mechanical properties including liquid-to-solid transition of hydrogels. These stimuli-responsive smart hydrogels have received significant attention because of human-related uses including food,[24] cosmetics,[25] controlled drug and cell delivery,[26−29] and tissue engineering.[30−34]

Along with the liquid-to-solid transition, both injectability and self-healing of the hydrogels are some of the most crucial viscoelastic properties for potential biorelated applications.[21,35] For the ABA triblock copolymer hydrogels, the viscoelastic characteristics are primarily governed by the kinetics of end-block pullout from the micellar cores (i.e., sticker lifetime) that is the underlying process to attain the stress (terminal) relaxation of the triblock copolymer hydrogels.[36,37] Recently, the gel relaxation dynamics obtained by dynamic mechanical measurement were compared to the chain exchange kinetics of diblock copolymer micelles measured by time-resolved small-angle scattering because the chain pullout perpendicular to the interface is responsible for both behaviors.[40,41] They suggested that the enthalpic barrier at the core−solvent interface (i.e., interfacial tension), the chain architecture, and the midblock conformation play a critical role in managing the chain pullout kinetics.

When the end-block cores are frozen in dynamics, the behavior of the hydrogels is essentially similar to chemically cross-linked hydrogels.[38,39] Previously, many amphiphilic block copolymers often experienced a frozen structure in aqueous solvents with extremely slow or hindered chain dynamics, which is attributed to the high interfacial tension between the end-block and solvent and relatively long end-block length.[42−45] However, the recent development of macro-

Received: August 21, 2020
Revised: October 6, 2020

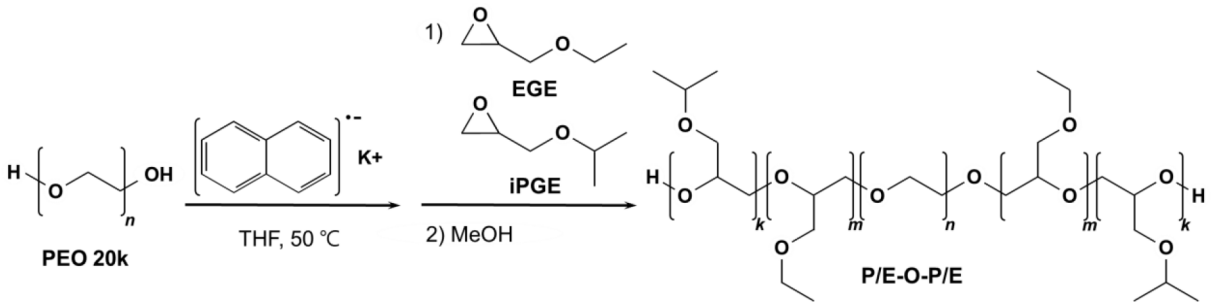

Figure 1. Synthetic scheme for ABA triblock copolymers.

molecular synthesis enables the managing of the chain pullout kinetics by introducing novel monomers exhibiting lower critical solution temperature (LCST) or upper critical solution temperature (UCST) behavior around room temperature in water.[8,9] Chassenieux et al. achieved the dynamic triblock copolymer hydrogel by adding hydrophilic monomers to lower the interfacial tension against water, and they observed that the viscoelastic characteristics are highly dependent on the end-block solubility.[17] In addition, Tsitsilianis et al. observed dynamic-to-frozen transition and injectability of polyacrylate-based ABA triblock copolymer hydrogels, which is attributed to the exponential temperature dependence of the sticker lifetime.[13] Recently, Nelson et al. explored direct-writing 3D printing materials using temperature- and shear-responsive hydrogels formed by A-PEO-A triblock copolymer hydrogels, where A block is poly(alkyl glycidyl ether) (PAGE).[21−23,46−48] As a PEO derivative, PAGE is highly biocompatible, and the LCST temperature is managed by copolymerization and side-chain structure.[9,49,50]

In this study, we address the hydrogel relaxation dynamics by systematically modifying end-block hydrophobicity and temperature at a fixed end-block length. The hydrogels were formed by ABA triblock copolymers in water, where B midblock is PEO and A end-block is the copolymers of poly(isopropyl glycidyl ether) (poly(iPGE)) and poly(ethyl glycidyl ether) (poly(EGE)) with the varying monomer ratio. Since both poly(iPGE) and poly(EGE) exhibit LCST behavior with different critical temperatures, copolymerization tunes the hydrophobicity of the end-block near room temperature.[23] All hydrogels show thermoresponsiveness with the tunable transition temperature, and small modification of the end-block structure produces considerable change in the relaxation time. Based on the facile dynamics, the injectability and self-healing property of the hydrogels were examined by direct-writing 3D printing. All polyether-based hydrogels showed biocompatibility and injectability, resulting in promising soft materials for biological and biomedical applications. Our findings shed a new light on understanding the critical factors in the relaxation of block copolymer hydrogels and their potential applications in various fields.

EXPERIMENTAL SECTION

Materials. Poly(ethyl glycidyl ether-*co*-isopropyl glycidyl ether-*b*-ethylene oxide-*b*-ethyl glycidyl ether-*co*-isopropyl glycidyl ether) ABA triblock copolymers were synthesized by anionic ring-opening polymerization of ethyl glycidyl ether and isopropyl glycidyl ether initiating from poly(ethylene oxide) (PEO, M_n 20 kDa, Sigma-Aldrich) macroinitiator as shown in Figure 1. Both ethyl glycidyl ether (EGE, TCI) and isopropyl glycidyl ether (iPGE, TCI) were degassed through three freeze−pump−thaw cycles and purified with butyl magnesium chloride for 2 h. Tetrahydrofuran (THF), a solvent, was collected from a dry solvent system. Potassium naphthalenide was prepared by mixing potassium metal and naphthalene in dry THF for at least 24 h. Under an argon atmosphere, the potassium naphthalenide solution was injected dropwise into a reactor filled with PEO macroinitiator in dry THF until a green color was retained. Subsequently, EGE and iPGE monomers mixture was added to obtain random copolymer of EGE and iPGE as the end-block and polymerized for at least 24 h at 50 °C.[21,50] Degassed methanol was injected into the reactor to terminate the polymerization. The triblock copolymers were then recovered by precipitation in diethyl ether.

The polymers were characterized by size exclusion chromatography (SEC, JASCO) and ^{1}H nuclear magnetic resonance spectroscopy (^{1}H NMR, Unity-Inova 500) as shown in Figure S1 and Figure S2. The molecular weight of the end-block and the EGE fraction, f_{EGE}, in one end-block were determined using a combination of ^{1}H NMR spectroscopy and the molecular weight of the initiated PEO block. SEC was used to provide the overall polydispersity index ($Đ = M_w/M_n$) of all triblock copolymers. Molecular characteristics of the triblock copolymers are provided in Table 1.

Table 1. Characterizations of the ABA Triblock Copolymer Prepared in This Study

polymer	M_{nPEO} (kg/mol)	$M_{n,end\text{-}block}$ [a] (kg/mol)	f_{EGE} [b]	N_{EGE} [c]	N_{iPGE} [d]	$Đ$
PEO	20	–	–	–	–	1.06
E_{26}−O−E_{26}	20	2.8	1.00	26	–	1.06
$P_{17}E_{11}$−O−$P_{17}E_{11}$	20	3.0	0.40	11	17	1.05
$P_{16}E_9$−O−$P_{16}E_9$	20	2.8	0.35	9	16	1.02
$P_{20}E_5$−O−$P_{20}E_5$	20	2.8	0.21	5	20	1.04
P_{26}−O−P_{26}	20	3.0	0.00	–	26	1.04

[a] M_n of one end-block. [b] Fraction of EGE monomers in the end-block. [c] Degree of polymerization of EGE monomers in one end-block. [d] Degree of polymerization of iPGE monomers in one end-block.

The monomer sequence of the copolymerization follows the reactivity of monomers and thus depends on both the steric effect and electronic properties. For the oxyanionic ring-opening polymerization of alkylene oxides, the density functional theory (DFT) calculation revealed the lower transition energy barrier for the sterically hindered glycidyl ether to the growing chain because of better coordination to the counterion.[51] Furthermore, the bulky substituents of glycidyl ethers show little or no influence on the reactivity

https://dx.doi.org/10.1021/acs.macromol.0c01939
Macromolecules XXXX, XXX, XXX−XXX

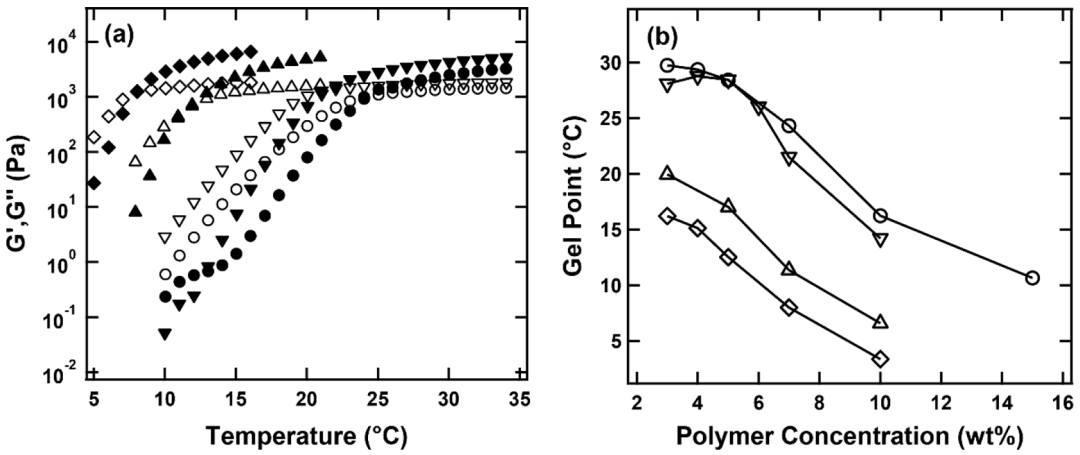

Figure 2. (a) Temperature-dependent moduli of G' (solid) and G'' (open) for 7 wt % polymer solutions of $P_{17}E_{11}$−O−$P_{17}E_{11}$ (●, ○), $P_{16}E_9$−O−$P_{16}E_9$ (▼, ▽), $P_{20}E_5$−O−$P_{20}E_5$ (▲, Δ), and P_{26}−O−P_{26} (◆, ◇). (b) Gel temperature, T_{gel}, as a function of polymer concentration for $P_{17}E_{11}$−O−$P_{17}E_{11}$ (○), $P_{16}E_9$−O−$P_{16}E_9$ (▽), $P_{20}E_5$−O−$P_{20}E_5$ (Δ), and P_{26}−O−P_{26} (◇) hydrogels.

ratio for the oxyanionic ring-opening polymerization.[52−54] Since iPGE monomers have one more methyl group at the end of the side chain than EGE monomers, the reactivity ratios are nearly identical, which provides a statistical random copolymerization of EGE and iPGE monomers.[23]

Polymer solutions were prepared by dissolving the appropriate amount of triblock copolymers in an aqueous solution, followed by annealing at 5 °C for at least 24 h using a Peltier temperature controller. Then, the solutions were heated to room temperature slowly.

Rheology. Rheological measurements were carried out on an MCR 302 rheometer (Anton Paar) equipped with a parallel plate of 25 mm in diameter. Temperature was controlled between 5 and 35 °C by a Peltier accessory. To avoid water evaporation from the samples, the fixture assembly was surrounded by a homemade acrylic cover, and water droplets were distributed inside the cover. Polymer solutions were loaded on a lower plate at low temperature, and the gap distance of 1 mm between upper and lower plates was maintained. Temperature dependences of G' and G'' were measured to obtain the gelation temperature with a frequency of 6.28 rad/s (=1 Hz), a strain of 0.1%, and a ramping rate of 1 °C/min. Gelation temperature, T_{gel}, was determined as the temperature where G' and G'' intersect.[55] Dynamic frequency sweeps were examined in the linear viscoelastic regime (ca. 0.1% strain) at several temperatures, and then the master curve was obtained by time−temperature superposition (tTS) principle along the frequency axis with small variation in vertical shift. The longest relaxation times were identified by the point where G' and G'' intersect in the master curve. Cyclic oscillatory strain measurement was performed at 30 °C using an alternating strain of 0.5% and 100% with a frequency of 6.28 rad/s.

Small-Angle X-ray Scattering (SAXS). SAXS experiments were performed on beamline 4C SAXS II at Pohang Acceleration Laboratory (PAL) using 16.9 keV radiation corresponding to a wavelength of λ = 0.734 Å.[56] The sample-to-detector distance was 4 m, which covers 0.007 Å^{-1} < q < 0.12 Å^{-1}, where q is a wave vector defined as $q = 4\pi\lambda^{-1}\sin(\theta/2)$. Temperature was controlled by the combination of an electric heater and a fluid circulating system. Specimens were loaded in sealed capillaries, followed by X-ray exposure for 5 s after 5 min annealing at a target temperature. Two-dimensional SAXS images, collected using a MAR-CCD detector, were azimuthally averaged to one-dimensional plots of intensity, $I(q)$, versus q.

Cell Viability. A cell viability test was performed by mouse fibroblast cells (L929) purchased from the Korean Cell Line Bank (Seoul, Korea). L929 cells were seeded in 96-well plates at a density of 7 × 10^3 cells per well and cultured for 24 h in a CO_2 incubator (5% CO_2 at 37 °C). The culture medium Rosewell Park Memorial Institute (RPMI) 1640 was used with 25 mM sodium bicarbonate, 10% fetal bovine serum, and 1% penicillin−streptomycin. After the culture medium was removed, each well was washed with 1× phosphate buffer saline (PBS). Each well was then filled with 90 μL of fresh media and 10 μL of various concentrations of polymer solutions and incubated for an additional 24 h. For the assessment of cell viability, each well was washed with PBS and filled with 10 μL of thiazolyl blue tetrazolium bromide (MTT, Sigma-Aldrich) stock solution (5 mg/mL) and 90 μL of fresh media. After incubation for 4 h, 200 μL of DMSO was added to each well to dissolve the MTT-formazan crystal, and the plates were gently stirred for 15 min. UV absorbance was recorded at a wavelength of 540 and 620 nm for the formazan crystals and the reference, respectively, by microplate reader (Infinite 200 pro, Tecan)

RESULTS AND DISCUSSION

When ABA triblock copolymers are dissolved in an aqueous solvent, hydrophobic A blocks aggregate into cores, and hydrophilic B blocks form a bridge between cores or a loop. In this study, the hydrophilicity of the A end-block was controlled by the random copolymerization of ethyl glycidyl ether (EGE) and isopropyl glycidyl ether (iPGE) monomers with a fixed overall degree of polymerization of 25−28. Poly(EGE) homopolymers exhibit the lower critical solution temperature (LCST) behavior with the critical temperature of ∼15 °C for 1 wt % aqueous solution, whereas poly(iPGE) homopolymers are insoluble.[23,49,50] Thus, random copolymerization of EGE and iPGE tunes the critical temperature as a function of the fraction of EGE monomers, f_{EGE}, within a copolymer.[57,58]

The critical micelle concentration, CMC, of the triblock copolymer solutions at room temperature using the fluorescent probe of pyrene gradually increases as f_{EGE} increases, reflecting that the end-block becomes more hydrophilic and shows the

https://dx.doi.org/10.1021/acs.macromol.0c01939
Macromolecules XXXX, XXX, XXX−XXX

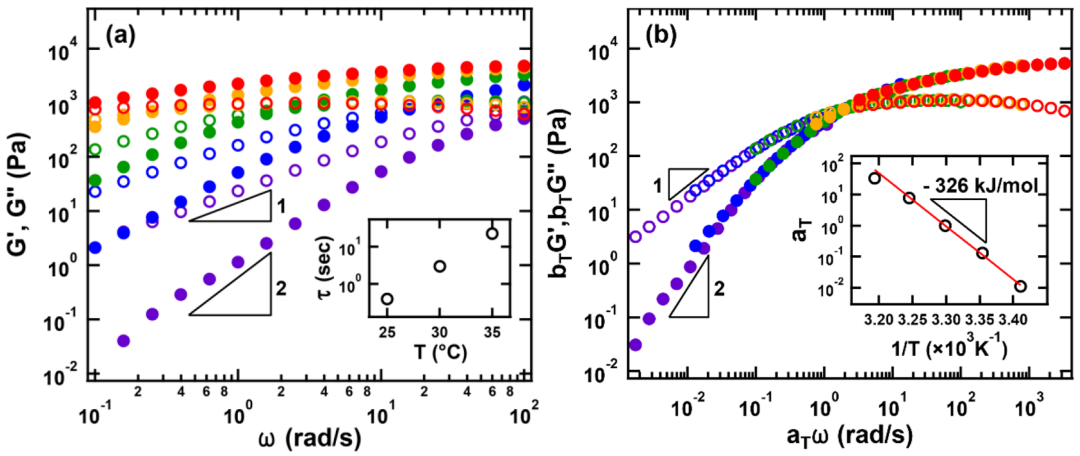

Figure 3. (a) Frequency dependence of G' (solid symbol) and G'' (open symbol) for 5 wt % $P_{16}E_9$−O−$P_{16}E_9$ hydrogels at 20 (purple), 25 (blue), 30 (green), 35 (yellow), and 40 °C (red). The inset shows the temperature-dependent relaxation time, τ. (b) Time−temperature superposition master curve at the reference temperature of 30 °C. The inset shows the temperature dependence of the horizontal shift factor, a_T; Arrhenius analysis provides the apparent activation energy of −326 kJ/mol.

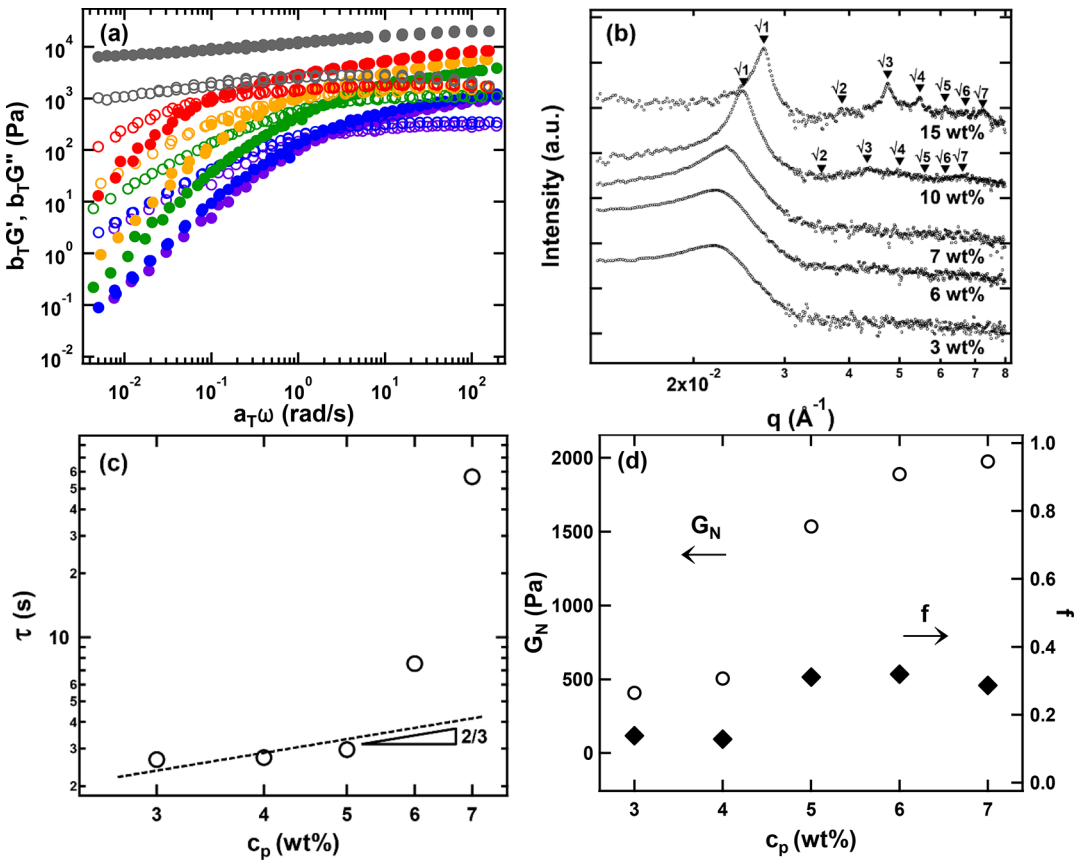

Figure 4. (a) Time−temperature superposition master curve of G' (filled) and G'' (open) for $P_{16}E_9$−O−$P_{16}E_9$ at 3 (purple), 4 (blue), 5 (green), 6 (yellow), 7 (red), and 10 wt % (gray) at the reference temperature of 30 °C. (b) SAXS profiles for $P_{16}E_9$−O−$P_{16}E_9$ hydrogels as a function of polymer concentration at 30 °C. Data are vertically shifted for clarity. (c) Polymer concentration dependence of the relaxation time, τ. (d) Polymer concentration dependence of the plateau moduli, G_N, and the corresponding fraction of elastically effective chain, f.

higher critical temperature at higher f_{EGE} (see the Supporting Information). In addition, the hydrophobicity of the end-block is estimated by the log P value, where P is the ratio of the concentration of a solute between water and octanol.[59] The log P values of end-block gained by the ALOGPS 2.1 program are 2.90, 2.99, 3.12, and 3.30 for $P_{17}E_{11}$−O−$P_{17}E_{11}$, $P_{16}E_9$−O−$P_{16}E_9$, $P_{20}E_5$−O−$P_{20}E_5$, and P_{26}−O−P_{26}, indicating that the end-block is more hydrophilic with increasing f_{EGE}.[60] For comparison, log P for poly(propylene oxide) of similar chain length was calculated as 4.71.

All triblock copolymer solutions examined between 3 and 10 wt % were prepared by complete dissolution of the polymers in water at 5 °C, followed by heating to room temperature slowly, which provides reproducible self-assembled structures. Figure 2a shows the temperature dependence of the storage modulus, G', and the loss modulus, G'', for 7 wt % aqueous solutions of

https://dx.doi.org/10.1021/acs.macromol.0c01939
Macromolecules XXXX, XXX, XXX−XXX

P_{26}−O−P_{26}, $P_{20}E_5$−O−$P_{20}E_5$, $P_{16}E_9$−O−$P_{16}E_9$, and $P_{17}E_{11}$−O−$P_{17}E_{11}$. At a lower temperature, liquidlike behavior was observed (i.e., $G' < G''$), whereas G' becomes dominant over G'' (i.e., $G' > G''$) as temperature increases. The gelation temperature, T_{gel}, identified as the temperature where G' and G'' intersect, is 8, 11, 22, and 24 °C for P_{26}−O−P_{26}, $P_{20}E_5$−O−$P_{20}E_5$, $P_{16}E_9$−O−$P_{16}E_9$, and $P_{17}E_{11}$−O−$P_{17}E_{11}$ solutions at 7 wt %, respectively. E_{26}−O−E_{26} polymer solutions are liquidlike and do not show the sol-to-gel transition between 5 and 35 °C. The elevated T_{gel} is primarily attributed to the higher critical temperature of the end-blocks with larger f_{EGE}, which shows good agreement with the previous report.[23]

Overall T_{gel} as a function of the polymer concentration for P_{26}−O−P_{26}, $P_{20}E_5$−O−$P_{20}E_5$, $P_{16}E_9$−O−$P_{16}E_9$, and $P_{17}E_{11}$−O−$P_{17}E_{11}$ is illustrated in Figure 2b, which denotes that T_{gel} gradually decreases with increasing polymer concentration as well as reducing f_{EGE}. Temperature-dependent moduli for all polymer solutions are shown in Figure S5. The polymer concentration dependence of T_{gel} is consistent with the previous findings for the thermoresponsive hydrogels induced by poly(alkyl glycidyl ether)-based polymers, methacrylate-based terpolymers, and Pluronics.[22,23,61,62] The strong dependence of T_{gel} on the polymer concentration is still an open question and potentially related to two thermodynamic factors: (1) a polymer concentration dependence of the interaction parameter[63] and (2) strong interaction between end-block and aqueous media.[64] Ogura et al. reported that the critical temperature of the poly(EGE) in water shows strong dependence on the polymer concentration, yet is nearly irrespective of the molecular weight.[65] Besides, Lee et al. observed an unusual LCST behavior of PEO in ionic liquids, in which the phase diagram is either roughly symmetric or asymmetric with a critical point shifted to a higher PEO concentration. They proposed that strong interaction between PEO and the ionic liquid, such as hydrogen bonding, plays a significant role in this unusual behavior.[64,66,67]

Figure 3a depicts the frequency sweep of G' and G'' for 5 wt % $P_{16}E_9$−O−$P_{16}E_9$ hydrogels at various temperatures between 20 and 40 °C. At a higher temperature, G' is larger than G'' over the measured frequency range between 0.1 and 100 rad/s, which indicates a rubberlike solid behavior. As the temperature decreases, a crossover frequency of G' and G'', ω_c, appears and shifts toward a higher frequency. At a lower temperature, the power law exponent of G' and G'' on frequency is close to 2 and 1, respectively, reflecting the terminal relaxation behavior. Here, the longest relaxation time, τ, is defined as the inverse of ω_c as $\tau = 2\pi/\omega_c$. The characteristic τ is 0.39, 3.0, and 23 s for 25, 30, and 35 °C, respectively, as shown in the inset of Figure 3a, indicating the steep decrease in the dynamics within 10 °C, consistent with the previous findings.[13,68]

Based on the frequency sweep results, the master curve of $b_T G'$ and $b_T G''$ against $a_T\omega$ for 5 wt % $P_{16}E_9$−O−$P_{16}E_9$ hydrogels was constructed by time−temperature superposition (tTS) principles as shown in Figure 3b. All data were horizontally shifted to overlap tan δ, defined as tan $\delta = G''/G'$, and then followed by a vertical shift to overlap G' values. The applicability of tTS suggests that the underlying origin of the hydrogel viscoelastic behavior does not change over the temperature range studied. The corresponding horizontal shift factor, a_T, was recorded as shown in the inset of Figure 3b, which shows a linear relationship between $\ln(a_T)$ and $1/T$ within the temperature range investigated. Using Arrhenius analysis, the apparent activation energy, ΔH_{app}, was estimated as −326 kJ/mol. The negative value is consistent with the previous findings for the LCST system, which will be discussed further later.[13,37,68]

Figure 4a illustrates the polymer concentration, c_p, dependence of the tTS master curves for $P_{16}E_9$−O−$P_{16}E_9$ at 3, 4, 5, 6, 7, and 10 wt % at a reference temperature of 30 °C. The temperature-dependent a_T for measured concentrations is nearly overlapped as shown in Figure S6, deducing that the apparent activation energy is nearly identical. As c_p increases, the frequency at the crossover point, ω_c, moves to lower frequency, and the plateau modulus, G_N, is intensified. At low frequency, almost all polymer solutions show the terminal relaxation behavior as $G' \sim \omega^2$ and $G'' \sim \omega^1$. However, at 10 wt % solution the terminal behavior was not observed, and the ω_c disappears, which is attributed to the formation of a body-centered cubic structure.[41,69,70]

SAXS data for the $P_{16}E_9$−O−$P_{16}E_9$ hydrogel at various polymer concentrations at 30 °C are displayed in Figure 4b. Because of the small difference in electron density of the polyether-based block against water, the SAXS intensity is relatively weak. The structure peak near $q \sim 0.025$ Å^{-1} is responsible for the average distance between end-block cores, and the distance decreases as the concentration increases. Above 10 wt % solution, Bragg peaks are evolved with peak ratios, q/q^*, of $1:\sqrt{2}:\sqrt{3}:\sqrt{5}:\sqrt{6}:\sqrt{7}$, which is attributed to the fact that the cores are packed on a body-centered cubic (bcc) lattice.

The polymer concentration dependence of τ is illustrated in Figure 4c at the reference temperature of 30 °C, where τ increases with increasing c_p. The abrupt increase in τ above 6 wt % presumably reflects a verge of congested micellar cores where the cores cannot easily flow.[71] As c_p increases, τ is predicted to increase because (1) the distance between micellar junctions decreases, and thus the thermodynamically destabilized PEO midblocks can be relaxed, and (2) the crowdedness in the matrix increases (i.e., corona screening).[36,41,72−74] Previously, Ianniruberto et al. predicted $\tau \sim c_p^{2/3}$ for the homogeneous network formed by telechelic associating polymers, in which a sequence of detachment for the end-block relaxation of the dynamic network was postulated.[74] The prediction showed good agreement with the previous observation with the hydrophobically modified ethoxylated urethanes hydrogels.[75,76] Recently, Zinn et al. however observed $\tau \sim c_p^1$ for triblock copolymer hydrogel where PEO is capped by alkyl chain on both sides, and they proposed that midblock conformation plays a significant role in the relaxation process.[40] Ye et al. reported $\tau \sim c_p^{7.6}$ for methacrylate-based triblock copolymer gels in dimethylformamide (DMF) and proposed that the significant c_p dependence is attributed to the concentration-dependent connectivity of the network.[55]

Figure 4d depicts the plateau moduli, G_N, as a function of c_p at the reference temperature 30 °C. Since G' values do not show a complete horizontal plateau, G_N was estimated to be two times the modulus at ω_c based on the Maxwell model.[55,77] Since elastically active chains contribute to the rubber elasticity in the rheological measurement, the fraction of elastically active chain, f, can be calculated by $G_N = f\nu_0 kT$, where ν_0, k, and T are the number density of midblocks, Boltzmann constant, and absolute temperature, respectively. The value of f shows a steep increase at 5 wt %, followed by a slight decrease up to 7 wt %, which indicates that the relaxation time is not dependent on the connectivity in our system.

https://dx.doi.org/10.1021/acs.macromol.0c01939
Macromolecules XXXX, XXX, XXX−XXX

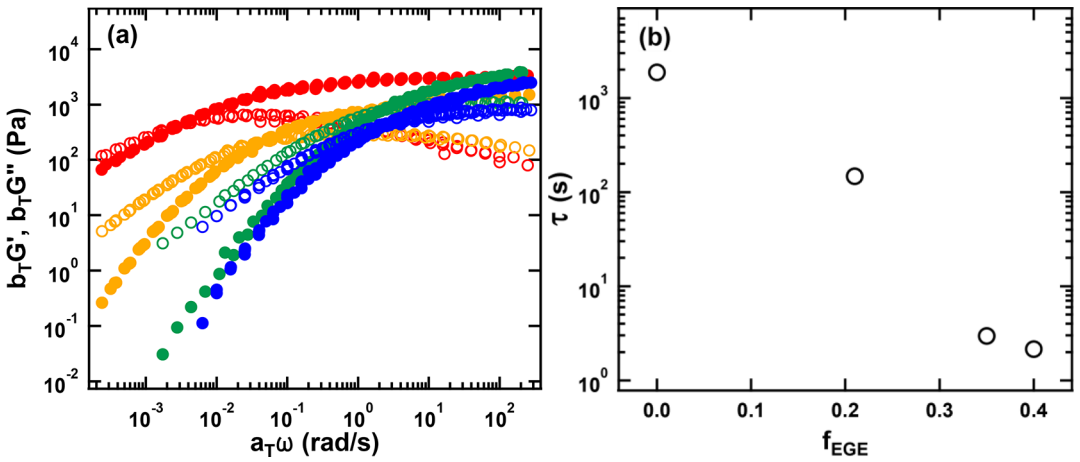

Figure 5. (a) Time−temperature superposition master curve of G' (filled) and G'' (open) for 5 wt % solutions of P_{26}−O−P_{26} (red), $P_{20}E_5$−O−$P_{20}E_5$ (yellow), $P_{16}E_9$−O−$P_{16}E_9$ (green), and $P_{17}E_{11}$−O−$P_{17}E_{11}$ (blue) at the reference temperature of 30 °C. (b) Relaxation time, τ, as a function of the hydrophobicity of the end-block, f_{EGE}.

Figure 5a displays the tTS master curves for 5 wt % solutions of P_{26}−O−P_{26}, $P_{20}E_5$−O−$P_{20}E_5$, $P_{16}E_9$−O−$P_{16}E_9$, and $P_{17}E_{11}$−O−$P_{17}E_{11}$ at the reference temperature of 30 °C, where the end-block hydrophobicity progressively decreases with the fixed overall degree of polymerization of 25−28. All curves show a rubberlike behavior at higher frequency, followed by the terminal relaxation at lower frequency. As f_{EGE} increases, ω_c shifts to higher frequency, while G_N is nearly identical. This reflects that the hydrogel structure is primarily maintained, but the relaxation dynamics are regulated by the end-block property.

Based on ω_c, the relaxation time, τ, for polymer solution of P_{26}−O−P_{26}, $P_{20}E_5$−O−$P_{20}E_5$, $P_{16}E_9$−O−$P_{16}E_9$, and $P_{17}E_{11}$−O−$P_{17}E_{11}$ at 5 wt % was computed as 1.9×10^2, 2.1×10, 3.0, and 2.2 s, respectively, as illustrated in Figure 5b. It is surprising that a small modification of the mixing ratio of ethyl glycidyl ether (EGE) and isopropyl glycidyl ether (iPGE) in the end-block results in significantly slower dynamics by 2 orders of magnitude. Here, we note that the end-block pullout from the cores is required for the terminal relaxation of the triblock copolymer hydrogel, and thus the measured τ should correspond to or be larger than the end-block chain pullout time, $\tau_{pullout}$, as shown in Figure 6.[40,41,75,78] Note that the effect of the congested micellar cores was not significant for all 5 wt % hydrogels. Regarding the relaxation dynamics of triblock copolymer hydrogels, Peters et al. proposed that τ observed by rheological measurement is identified with the chain end pullout time, $\tau_{pullout}$, which is associated with the Rouse dynamics of the end-blocks in the cores and the thermodynamic barrier at the core−solvent interface.[41] Considering the entanglement degree of the polymerization molecular weight of PEO of 1.6×10^3 g/mol that corresponds to $N = 36$, the random copolymer of poly(EGE) and poly(iPGE) of N_{end} = 25−28 indicates that the end-blocks are not entangled in the cores.[79] Also, the monomeric friction factors, ζ, for both poly(EGE) and poly(iPGE) are expected to be nearly identical because of similar molecular structure and nearly identical glass transition temperature of −66 °C.[80] Therefore, the Rouse relaxation in the cores can occur at a comparable time scale for all polymer hydrogels at 30 °C, resulting in that the huge difference in the τ is attributed to the thermodynamic penalty of the chain extraction from the micellar cores.

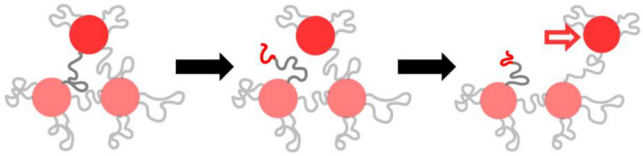

Figure 6. Schematic illustration of the relaxation process for ABA triblock copolymer hydrogel. The end-block chain pullout is required for the terminal relaxation detected by rheological measurement.

In more detail, Peters et al. proposed that $\tau_{pullout}$ was modeled as $\tau_{pullout} = \tau_{Rouse} \times \exp[\alpha\chi N_{end}]$, where α, χ, and N_{end} are an unknown $O(1)$ prefactor, the Flory−Huggins interaction parameter, and the degree of polymerization of the end-block, respectively.[41,45] The $\alpha\chi N_{end}$ denotes the thermodynamic penalty in kT unit to the chain pullout at the interface due to the unfavorable monomer−solvent contact.[81] Here, τ_{Rouse} is the longest Rouse relaxation time, defined as $\tau_{Rouse} = (b^2 N_{end}{}^2\zeta)/(6\pi^2 kT)$, where b, ζ, k, and T are the statistical segment length, the monomeric friction factor, the Boltzmann constant, and the absolute temperature, respectively. In our system, b was taken as b = 6.0 Å similar to PEO, and ζ for all polymers was estimated as 1.94×10^{-10} kg/s at 30 °C based on the zero-shear viscosity measurement for poly(iPGE) as shown in Figure S8. Therefore, $\alpha\chi$ was calculated as 0.68, 0.75, 0.89, and 0.92 for $P_{17}E_{11}$−O−$P_{17}E_{11}$, $P_{16}E_9$−O−$P_{16}E_9$, $P_{20}E_5$−O−$P_{20}E_5$, and P_{26}−O−P_{26}, respectively, at 30 °C. As a comparison, χ between poly(propylene oxide) (PPO) and water, $\chi_{PPO/water}$, was estimated as 2.1 using activity data on PPO aqueous solution.[82,83] It is pointed out that the interfacial energy barrier between poly(alkyl glycidyl ether) and aqueous media is considerably intensified with a few more methyl groups. Aoki et al. presented that the LCST critical temperature is significantly affected by the side-chain structure such as methyl, ethyl, and butyl group of poly(alkyl glycidyl ether) in water.[50] Similarly, Isono et al. showed that the critical temperature in water is highly dependent on the side-chain structure such as the number of oxyethylene units and the terminal alkyl group of the poly(alkyl glycidyl ether) in a systematic way.[49] Song et al. also showed that the cyclic side chain provides much lower critical temperature than its acyclic analogue of poly(alkyl glycidyl ether) in water.[84]

https://dx.doi.org/10.1021/acs.macromol.0c01939
Macromolecules XXXX, XXX, XXX−XXX

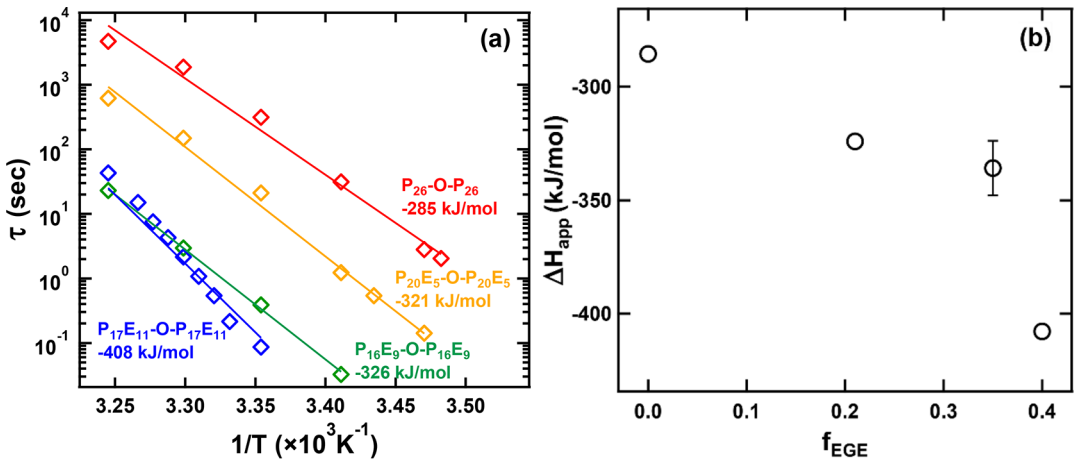

Figure 7. (a) Relaxation time as a function of temperature for $P_{17}E_{11}$−O−$P_{17}E_{11}$ (blue), $P_{16}E_9$−O−$P_{16}E_9$ (green), $P_{20}E_5$−O−$P_{20}E_5$ (yellow), and P_{26}−O−P_{26} (red) at 5 wt %. Solid lines are Arrhenius plots, which provide the apparent activation energy. (b) Apparent activation energy as a function of f_{EGE} for 5 wt % hydrogels. In the case of $P_{16}E_9$−O−$P_{16}E_9$, the activation energy was obtained from 3−7 wt % solutions.

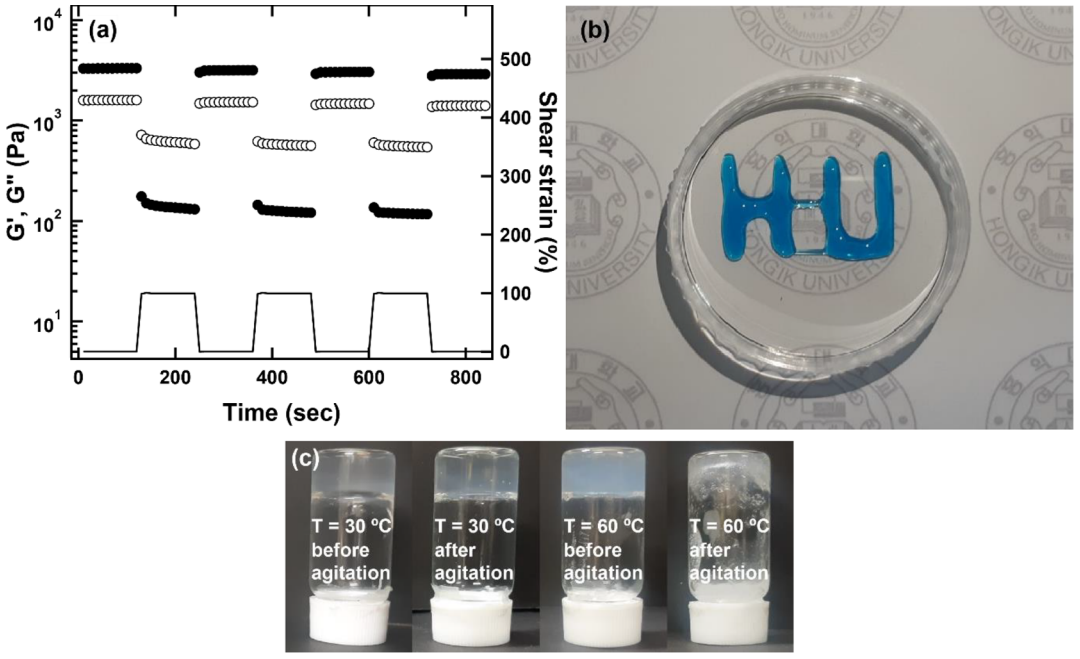

Figure 8. (a) Cyclic oscillatory strain experiment for 7 wt % $P_{16}E_9$−O−$P_{16}E_9$ hydrogel at 30 °C upon periodic oscillatory strain between 0.5% and 100%, indicating the reversible shear responsiveness. (b) Direct-write 3D printed structure of 7 wt % $P_{16}E_9$−O−$P_{16}E_9$ hydrogel where three layers were stacked. (c) Hydrogel photos before and after severe agitation by a vortex mixer for 7 wt % $P_{20}E_5$−O−$P_{20}E_5$ hydrogels at 30 and 60 °C.

Temperature-dependent τ was computed by a_T for P_{26}−O−P_{26}, $P_{20}E_5$−O−$P_{20}E_5$, $P_{16}E_9$−O−$P_{16}E_9$, and $P_{17}E_{11}$−O−$P_{17}E_{11}$ at 5 wt % as displayed in Figure 7a. As discussed above, the temperature dependence of $\tau_{pullout}$ is mainly dictated by ζ and χ, where ζ is decreasing, yet χ is increasing with increasing temperature for the LCST system.[85] Then, $\alpha\chi$ was estimated as 0.45, 0.57, 0.67, and 0.76 for 20, 25, 30, and 35 °C for 5 wt % $P_{16}E_9$−O−$P_{16}E_9$ solutions as shown in Figure S7, indicating that the significant increment of the unfavorable interaction occurs with a small increase in temperature. Therefore, a sequence of complete dissolution and dynamics to frozen hydrogel primarily originates from a considerable temperature-dependent thermodynamic property.

As an alternative analysis to gain thermodynamic insight, the apparent activation energy, ΔH_{app}, was obtained by the Arrhenius equation as $\tau = \tau_0 \exp[\Delta H_{app}/RT]$, where τ_0 is the attempt time.[13,40,68] As f_{EGE} increases (more hydrophilic), ΔH_{app} becomes more negative as shown in Figure 7b. The negative value of ΔH_{app} represents the enthalpy change for the removal of an end-block from the cores and hydration of EGE or iPGE to solubilize for the LCST system.[37] Onoda et al. observed that the introduction of hydrophobic monomer to the end-block provides less negative ΔH_{app} for LCST-type triblock copolymer hydrogels, which is consistent with our result.[68]

Figure 8a displays the cyclic oscillatory strain measurement for 7 wt % $P_{16}E_9$−O−$P_{16}E_9$ hydrogel at 30 °C, where the hydrogels exhibit liquidlike behavior at high strain, followed by rapid recovery to solidlike behavior at low strain. The reversible shear-responsiveness and the dynamic associative junction are required for the extrusion-based 3D printing. Figure 8b shows the printed structure of three layers using a

https://dx.doi.org/10.1021/acs.macromol.0c01939
Macromolecules XXXX, XXX, XXX−XXX

homemade direct-write printer, in which buckling of the layered structure was not observed. Relatively faster relaxation process and chain exchange endow rapid adhesion between layers and thus self-healing property. However, as the relaxation becomes slower the unique viscoelastic characteristics of the hydrogels were nearly vanished. As a representative example, severe agitation by a vortex mixer results in fracture into small pieces for 7 wt % $P_{20}E_5-O-P_{20}E_5$ hydrogels at 60 °C as shown in Figure 8c, which stresses that the relaxation process plays a significant role in the viscoelastic characteristics.

All polymer hydrogels show good cell viability of 99%, 88%, and 94% at a high concentration of 2500 μg/mL for $P_{17}E_{11}-O-P_{17}E_{11}$, $P_{20}E_5-O-P_{20}E_5$, and $P_{26}-O-P_{26}$ hydrogels, respectively, as shown in Figure S9. The results of *in vitro* MTT assay using mouse fibroblast cells (L929) indicate that the polymer hydrogels are biocompatible, which is consistent with the results obtained by Fellin et al. using HeLa cells.[23] The low cytotoxicity associated with the unique viscoelastic behavior of the polyether-based hydrogels potentially opens new insights for the thermoresponsive polymers and the potential materials for the biological and biomedical applications.

SUMMARY

We investigated the relaxation dynamics of biocompatible and injectable triblock copolymer hydrogels as a function of temperature and end-block hydrophobicity, regulated by the random copolymerization of ethyl glycidyl ether (EGE) and isopropyl glycidyl ether (iPGE). As the end-blocks become hydrophobic, (1) the sol−gel transition occurs at lower temperatures and lower polymer concentration, and (2) the hydrogel relaxation time is significantly slower. We observed that the small increment of hydrophobic moieties and/or higher temperature intensifies the unfavorable interaction of poly(alkyl glycidyl ether) against water significantly, suggesting that monomer design is of great importance for applications in aqueous media. In particular, chain relaxation dynamics govern the injectability and the self-healing property of the self-assembled triblock copolymer hydrogels. Besides, all the polyether-based ABA triblock copolymer hydrogels show less cytotoxicity, reflecting promising soft materials for biological and biomedical applications. Overall, the results advance the current understanding of how hydrogel dynamics are influenced by the molecular structure of poly(alkyl glycidyl ether) in aqueous solvents and should give assistance to design complex fluids obtained by polyether block copolymer.

ASSOCIATED CONTENT

Supporting Information

The Supporting Information is available free of charge at https://pubs.acs.org/doi/10.1021/acs.macromol.0c01939.

Additional analysis including SEC traces and NMR spectroscopy of the synthesized block copolymers, the critical micelle concentration measurement, SAXS measurement, and rheological measurement (PDF)

AUTHOR INFORMATION

Corresponding Author

Soo-Hyung Choi − *Department of Chemical Engineering, Hongik University, Seoul 04066, Republic of Korea;* orcid.org/0000-0002-4078-6285; Email: shchoi@hongik.ac.kr

Authors

Hyunjoon Jung − *Department of Chemical Engineering, Hongik University, Seoul 04066, Republic of Korea*

Seong-Eun Gang − *Department of Chemical Engineering, Hongik University, Seoul 04066, Republic of Korea*

Jung-Min Kim − *Department of Chemical Engineering, Hongik University, Seoul 04066, Republic of Korea*

Tae-Young Heo − *Department of Chemical Engineering, Hongik University, Seoul 04066, Republic of Korea*

Sangho Lee − *Department of Chemical Engineering, Hongik University, Seoul 04066, Republic of Korea*

Eeseul Shin − *Department of Chemistry, Yonsei University, Seoul 03722, Republic of Korea;* orcid.org/0000-0002-9774-2961

Byeong-Su Kim − *Department of Chemistry, Yonsei University, Seoul 03722, Republic of Korea;* orcid.org/0000-0002-6419-3054

Complete contact information is available at: https://pubs.acs.org/10.1021/acs.macromol.0c01939

Author Contributions

[§]These authors contributed equally to the work.

Notes

The authors declare no competing financial interest.

ACKNOWLEDGMENTS

This work was supported by the Samsung Research Foundation (SRFC-MA1602-07)

REFERENCES

(1) Raspaud, E.; Lairez, D.; Adam, M.; Carton, J. P. Triblock Copolymers in a Selective Solvent. 1. Aggregation Process in Dilute Solution. *Macromolecules* **1994**, *27*, 2956−2964.

(2) Semenov, A. N.; Joanny, J. F.; Khokhlov, A. R. Associating Polymers: Equilibrium and Linear Viscoelasticity. *Macromolecules* **1995**, *28*, 1066−1075.

(3) Lairez, D.; Adam, M.; Carton, J. P.; Raspaud, E. Aggregation of Telechelic Triblock Copolymers: From Animals to Flowers. *Macromolecules* **1997**, *30*, 6798−6809.

(4) Yu, L.; Zhang, H.; Ding, J. A Subtle End-Group Effect on Macroscopic Physical Gelation of Triblock Copolymer Aqueous Solutions. *Angew. Chem., Int. Ed.* **2006**, *45*, 2232−2235.

(5) Zhang, H.; Yu, L.; Ding, J. Roles of Hydrophilic Homopolymers on the Hydrophobic-Association-Induced Physical Gelling of Amphiphilic Block Copolymers in Water. *Macromolecules* **2008**, *41*, 6493−6499.

(6) Cui, S.; Yu, L.; Ding, J. Thermogelling of Amphiphilic Block Copolymers in Water: ABA Type Versus AB Or BAB Type. *Macromolecules* **2019**, *52*, 3697−3715.

(7) Mortensen, K.; Brown, W.; Joergensen, E. Phase Behavior of Poly(Propylene Oxide)-Poly(Ethylene Oxide)-Poly(Propylene Oxide) Triblock Copolymer Melt and Aqueous Solutions. *Macromolecules* **1994**, *27*, 5654−5666.

(8) Mihajlovic, M.; Staropoli, M.; Appavou, M.; Wyss, H. M.; Pyckhout-Hintzen, W.; Sijbesma, R. P. Tough Supramolecular Hydrogel Based on Strong Hydrophobic Interactions in a Multiblock Segmented Copolymer. *Macromolecules* **2017**, *50*, 3333−3346.

(9) Murakami, T.; Kawamori, T.; Gopez, J. D.; McGrath, A. J.; Klinger, D.; Saito, K. Synthesis of PEO-Based Physical Gels with Tunable Viscoelastic Properties. *J. Polym. Sci., Part A: Polym. Chem.* **2018**, *56*, 1033−1038.

(10) Chen, L.; Ci, T.; Yu, L.; Ding, J. Effects of Molecular Weight and its Distribution of PEG Block on Micellization and Thermogellability of PLGA−PEG−PLGA Copolymer Aqueous Solutions. *Macromolecules* **2015**, *48*, 3662−3671.
(11) Cui, S.; Yu, L.; Ding, J. Semi-Bald Micelles and Corresponding Percolated Micelle Networks of Thermogels. *Macromolecules* **2018**, *51*, 6405−6420.
(12) Lauber, L.; Santarelli, J.; Boyron, O.; Chassenieux, C.; Colombani, O.; Nicolai, T. pH- and Thermoresponsive Self-Assembly of Cationic Triblock Copolymers with Controlled Dynamics. *Macromolecules* **2017**, *50*, 416−423.
(13) Tsitsilianis, C.; Serras, G.; Ko, C.; Jung, F.; Papadakis, C. M.; Rikkou-Kalourkoti, M.; Patrickios, C. S.; Schweins, R.; Chassenieux, C. Thermoresponsive Hydrogels Based on Telechelic Polyelectrolytes: From Dynamic to "Frozen" Networks. *Macromolecules* **2018**, *51*, 2169−2179.
(14) Angelopoulos, S. A.; Tsitsilianis, C. Thermo-Reversible Hydrogels Based on Poly(N, N-Diethylacrylamide)-Block-Poly-(Acrylic Acid)-Block-Poly(N, N-Diethylacrylamide) Double Hydrophilic Triblock Copolymer. *Macromol. Chem. Phys.* **2006**, *207*, 2188−2194.
(15) Yu, L.; Chang, G.; Zhang, H.; Ding, J. Temperature-Induced Spontaneous Sol−gel Transitions of Poly(D, L-Lactic Acid-Co-Glycolic Acid)-B-Poly(Ethylene Glycol)-B-Poly(D, L-Lactic Acid-Co-Glycolic Acid) Triblock Copolymers and their End-Capped Derivatives in Water. *J. Polym. Sci., Part A: Polym. Chem.* **2007**, *45*, 1122−1133.
(16) Chen, L.; Ci, T.; Li, T.; Yu, L.; Ding, J. Effects of Molecular Weight Distribution of Amphiphilic Block Copolymers on their Solubility, Micellization, and Temperature-Induced Sol−Gel Transition in Water. *Macromolecules* **2014**, *47*, 5895−5903.
(17) Charbonneau, C.; Chassenieux, C.; Colombani, O.; Nicolai, T. Controlling the Dynamics of Self-Assembled Triblock Copolymer Networks Via the pH. *Macromolecules* **2011**, *44*, 4487−4495.
(18) Chang, G.; Yu, L.; Yang, Z.; Ding, J. A Delicate Ionizable-Group Effect on Self-Assembly and Thermogelling of Amphiphilic Block Copolymers in Water. *Polymer* **2009**, *50*, 6111−6120.
(19) Krogstad, D. V.; Lynd, N. A.; Choi, S.; Spruell, J. M.; Hawker, C. J.; Kramer, E. J.; Tirrell, M. V. Effects of Polymer and Salt Concentration on the Structure and Properties of Triblock Copolymer Coacervate Hydrogels. *Macromolecules* **2013**, *46*, 1512−1518.
(20) Dyakonova, M. A.; Berezkin, A. V.; Kyriakos, K.; Gkermpoura, S.; Popescu, M. T.; Filippov, S. K.; Štěpánek, P.; Di, Z.; Tsitsilianis, C.; Papadakis, C. M. Salt-Induced Changes in Triblock Polyampholyte Hydrogels: Computer Simulations and Rheological, Structural, and Dynamic Characterization. *Macromolecules* **2015**, *48*, 8177−8189.
(21) Zhang, M.; Vora, A.; Han, W.; Wojtecki, R. J.; Maune, H.; Le, A. B. A.; Thompson, L. E.; McClelland, G. M.; Ribet, F.; Engler, A. C.; Nelson, A. Dual-Responsive Hydrogels for Direct-Write 3D Printing. *Macromolecules* **2015**, *48*, 6482−6488.
(22) Karis, D. G.; Ono, R. J.; Zhang, M.; Vora, A.; Storti, D.; Ganter, M. A.; Nelson, A. Cross-Linkable Multi-Stimuli Responsive Hydrogel Inks for Direct-Write 3D Printing. *Polym. Chem.* **2017**, *8*, 4199−4206.
(23) Fellin, C. R.; Adelmund, S. M.; Karis, D. G.; Shafranek, R. T.; Ono, R. J.; Martin, C. G.; Johnston, T. G.; DeForest, C. A.; Nelson, A. Tunable Temperature- and Shear-Responsive Hydrogels Based on Poly(Alkyl Glycidyl Ether)S. *Polym. Int.* **2019**, *68*, 1238−1246.
(24) Zhang, H.; Zhang, F.; Yuan, R. In *Hydrogels Based on Natural Polymers*; Elsevier: Amsterdam, Netherlands, 2020; pp 357−410.
(25) Quattrone, A.; Czajka, A.; Sibilla, S. Thermosensitive Hydrogel Mask Significantly Improves Skin Moisture and Skin Tone; Bilateral Clinical Trial. *Cosmetics* **2017**, *4* (2), 17.
(26) Peppas, N.; Hilt, J.; Khademhosseini, A.; Langer, R. Hydrogels in Biology and Medicine: From Molecular Principles to Bionanotechnology. *Adv. Mater.* **2006**, *18* (11), 1345−1360.
(27) Burdick, J. A.; Prestwich, G. D. Hyaluronic Acid Hydrogels for Biomedical Applications. *Adv. Mater.* **2011**, *23*, 41.
(28) Yu, L.; Ding, J. Injectable Hydrogels as Unique Biomedical Materials. *Chem. Soc. Rev.* **2008**, *37*, 1473−1481.
(29) Ci, T.; Chen, L.; Yu, L.; Ding, J. Tumor Regression Achieved by Encapsulating a Moderately Soluble Drug into a Polymeric Thermogel. *Sci. Rep.* **2015**, *4*, 5473.
(30) Wang, H.; Heilshorn, S. C. Adaptable Hydrogel Networks with Reversible Linkages for Tissue Engineering. *Adv. Mater.* **2015**, *27*, 3717−3736.
(31) Kolesky, D. B.; Truby, R. L.; Gladman, A. S.; Busbee, T. A.; Homan, K. A.; Lewis, J. A. 3D Bioprinting of Vascularized, Heterogeneous Cell-Laden Tissue Constructs. *Adv. Mater.* **2014**, *26*, 3124−3130.
(32) Guillame-Gentil, O.; Semenov, O.; Roca, A. S.; Groth, T.; Zahn, R.; Vörös, J.; Zenobi-Wong, M. Engineering the Extracellular Environment: Strategies for Building 2D and 3D Cellular Structures. *Adv. Mater.* **2010**, *22*, 5443−5462.
(33) Rosales, A. M.; Anseth, K. S. The Design of Reversible Hydrogels to Capture Extracellular Matrix Dynamics. *Nature Reviews Materials* **2016**, *1*, 15012.
(34) Zhang, Z.; Lai, Y.; Yu, L.; Ding, J. Effects of Immobilizing Sites of RGD Peptides in Amphiphilic Block Copolymers on Efficacy of Cell Adhesion. *Biomaterials* **2010**, *31*, 7873−7882.
(35) Shi, H.; Ye, X.; Zhang, J.; Ye, J. Enhanced Osteogenesis of Injectable Calcium Phosphate Bone Cement Mediated by Loading Chondroitin Sulfate. *ACS Biomater. Sci. Eng.* **2019**, *5*, 262−271.
(36) Tanaka, F.; Edwards, S. F. Viscoelastic Properties of Physically Crosslinked Networks. 1. Transient Network Theory. *Macromolecules* **1992**, *25*, 1516−1523.
(37) Seitz, M. E.; Burghardt, W. R.; Faber, K. T.; Shull, K. R. Self-Assembly and Stress Relaxation in Acrylic Triblock Copolymer Gels. *Macromolecules* **2007**, *40*, 1218−1226.
(38) Zinn, T.; Willner, L.; Lund, R. Telechelic Polymer Hydrogels: Relation between the Microscopic Dynamics and Macroscopic Viscoelastic Response. *ACS Macro Lett.* **2016**, *5*, 1353−1356.
(39) Peters, A. J.; Lodge, T. P. Comparison of Gel Relaxation Times and End-Block Pullout Times in ABA Triblock Copolymer Networks. *Macromolecules* **2016**, *49*, 7340−7349.
(40) Tsitsilianis, C.; Iliopoulos, I.; Ducouret, G. An Associative Polyelectrolyte End-Capped with Short Polystyrene Chains. Synthesis and Rheological Behavior. *Macromolecules* **2000**, *33*, 2936−2943.
(41) Stavrouli, N.; Aubry, T.; Tsitsilianis, C. Rheological Properties of ABA Telechelic Polyelectrolyte and ABA Polyampholyte Reversible Hydrogels: A Comparative Study. *Polymer* **2008**, *49*, 1249−1256.
(42) Won, Y.; Davis, H. T.; Bates, F. S. Molecular Exchange in PEO-PB Micelles in Water. *Macromolecules* **2003**, *36*, 953−955.
(43) Jain, S.; Bates, F. S. Consequences of Nonergodicity in Aqueous Binary PEO-PB Micellar Dispersions. *Macromolecules* **2004**, *37*, 1511−1523.
(44) Lund, R.; Willner, L.; Stellbrink, J. ö; Lindner, P.; Richter, D. Logarithmic Chain-Exchange Kinetics of Diblock Copolymer Micelles. *Phys. Rev. Lett.* **2006**, *96*, 068302.
(45) Choi, S. H.; Lodge, T. P.; Bates, F. S. Mechanism of Molecular Exchange in Diblock Copolymer Micelles: Hypersensitivity to Core Chain Length. *Phys. Rev. Lett.* **2010**, *104*, 047802.
(46) Johnston, T. G.; Fellin, C. R.; Carignano, A.; Nelson, A. Poly(Alkyl Glycidyl Ether) Hydrogels for Harnessing the Bioactivity of Engineered Microbes. *Faraday Discuss.* **2019**, *219*, 58−72.
(47) Shafranek, R. T.; Leger, J. D.; Zhang, S.; Khalil, M.; Gu, X.; Nelson, A. Sticky Ends in a Self-Assembling ABA Triblock Copolymer: The Role of Ureas in Stimuli-Responsive Hydrogels. *Mol. Syst. Des. Eng.* **2019**, *4*, 91−102.
(48) Narupai, B.; Nelson, A. 100th Anniversary of Macromolecular Science Viewpoint: Macromolecular Materials for Additive Manufacturing. *ACS Macro Lett.* **2020**, *9*, 627−638.
(49) Isono, T.; Miyachi, K.; Satoh, Y.; Sato, S.; Kakuchi, T.; Satoh, T. Design and Synthesis of Thermoresponsive Aliphatic Polyethers with a Tunable Phase Transition Temperature. *Polym. Chem.* **2017**, *8*, 5698−5707.

https://dx.doi.org/10.1021/acs.macromol.0c01939
Macromolecules XXXX, XXX, XXX−XXX

(50) Aoki, S.; Koide, A.; Imabayashi, S.; Watanabe, M. Novel Thermosensitive Polyethers Prepared by Anionic Ring-Opening Polymerization of Glycidyl Ether Derivatives. *Chem. Lett.* **2002**, *31*, 1128−1129.
(51) Lee, B. F.; Wolffs, M.; Delaney, K. T.; Sprafke, J. K.; Leibfarth, F. A.; Hawker, C. J.; Lynd, N. A. Reactivity Ratios and Mechanistic Insight for Anionic Ring-Opening Copolymerization of Epoxides. *Macromolecules* **2012**, *45*, 3722−3731.
(52) Herzberger, J.; Niederer, K.; Pohlit, H.; Seiwert, J.; Worm, M.; Wurm, F. R.; Frey, H. Polymerization of Ethylene Oxide, Propylene Oxide, and Other Alkylene Oxides: Synthesis, Novel Polymer Architectures, and Bioconjugation. *Chem. Rev.* **2016**, *116*, 2170−2243.
(53) Mangold, C.; Wurm, F.; Obermeier, B.; Frey, H. Functional Poly(Ethylene Glycol)": PEG-Based Random Copolymers with 1,2-Diol Side Chains and Terminal Amino Functionality. *Macromolecules* **2010**, *43*, 8511−8518.
(54) Herzberger, J.; Leibig, D.; Liermann, J. C.; Frey, H. Conventional Oxyanionic Versus Monomer-Activated Anionic Copolymerization of Ethylene Oxide with Glycidyl Ethers: Striking Differences in Reactivity Ratios. *ACS Macro Lett.* **2016**, *5*, 1206−1211.
(55) Ye, Y. N.; Cui, K.; Indei, T.; Nakajima, T.; Hourdet, D.; Kurokawa, T.; Gong, J. P. Relaxation Dynamics and Underlying Mechanism of a Thermally Reversible Gel from Symmetric Triblock Copolymer. *Macromolecules* **2019**, *52*, 8651−8661.
(56) Kim, K. W.; Kim, J.; Yun, Y. D.; Ahn, H.; Min, B.; Kim, N. H.; Rah, S.; Kim, H. Y.; Lee, C. S.; Seo, I. D.; Lee, W. W.; Choi, H. J.; Jin, K. S. Small-Angle X-Ray Scattering Beamline BL4C SAXS at Pohang Light Source II. *Biodesign* **2017**, *5*, 24−29.
(57) Reinicke, S.; Schmelz, J.; Lapp, A.; Karg, M.; Hellweg, T.; Schmalz, H. Smart Hydrogels Based on Double Responsive Triblock Terpolymers. *Soft Matter* **2009**, *5*, 2648−2657.
(58) Heinen, S.; Rackow, S.; Schäfer, A.; Weinhart, M. A Perfect Match: Fast and Truly Random Copolymerization of Glycidyl Ether Monomers to Thermoresponsive Copolymers. *Macromolecules* **2017**, *50*, 44−53.
(59) Fujita, T.; Iwasa, J.; Hansch, C. A New Substituent Constant, Π, Derived from Partition Coefficients. *J. Am. Chem. Soc.* **1964**, *86*, 5175−5180.
(60) Kujawski, J.; Bernard, M. K.; Janusz, A.; Kuźma, W. Prediction of Log P: ALOGPS Application in Medicinal Chemistry Education. *J. Chem. Educ.* **2012**, *89*, 64−67.
(61) Ward, M. A.; Georgiou, T. K. Thermoresponsive Terpolymers Based on Methacrylate Monomers: Effect of Architecture and Composition. *J. Polym. Sci., Part A: Polym. Chem.* **2010**, *48*, 775−783.
(62) Constantinou, A. P.; Georgiou, T. K. Thermoresponsive Gels Based on ABC Triblock Copolymers: Effect of the Length of the PEG Side Group. *Polym. Chem.* **2016**, *7*, 2045−2056.
(63) Schäfer-Soenen, H.; Moerkerke, R.; Berghmans, H.; Koningsveld, R.; Dušek, K.; Šolc, K. Zero and Off-Zero Critical Concentrations in Systems Containing Polydisperse Polymers with very High Molar Masses. 2. the System Water-Poly(Vinyl Methyl Ether). *Macromolecules* **1997**, *30*, 410−416.
(64) de Gennes, P. G. Special Features of Water Soluble Polymers. *Pure Appl. Chem.* **1992**, *64*, 1585−1588.
(65) Ogura, M.; Tokuda, H.; Imabayashi, S.; Watanabe, M. Preparation and Solution Behavior of a Thermoresponsive Diblock Copolymer of Poly(Ethyl Glycidyl Ether) and Poly(Ethylene Oxide). *Langmuir* **2007**, *23*, 9429−9434.
(66) Lee, H.; Newell, N.; Bai, Z.; Lodge, T. P. Unusual Lower Critical Solution Temperature Phase Behavior of Poly(Ethylene Oxide) in Ionic Liquids. *Macromolecules* **2012**, *45*, 3627−3633.
(67) Lee, H.; Lodge, T. P. Lower Critical Solution Temperature (LCST) Phase Behavior of Poly(Ethylene Oxide) in Ionic Liquids. *J. Phys. Chem. Lett.* **2010**, *1*, 1962−1966.
(68) Onoda, M.; Ueki, T.; Tamate, R.; Akimoto, A. M.; Hall, C. C.; Lodge, T. P.; Yoshida, R. Precisely Tunable Sol−Gel Transition Temperature by Blending Thermoresponsive ABC Triblock Terpolymers. *ACS Macro Lett.* **2018**, *7*, 950−955.
(69) Kossuth, M. B.; Morse, D. C.; Bates, F. S. Viscoelastic Behavior of Cubic Phases in Block Copolymer Melts. *J. Rheol.* **1999**, *43*, 167−196.
(70) Sebastian, J. M.; Graessley, W. W.; Register, R. A. Steady-Shear Rheology of Block Copolymer Melts and Concentrated Solutions: Defect-Mediated Flow at Low Stresses in Body-Centered-Cubic Systems. *J. Rheol.* **2002**, *46*, 863−879.
(71) Park, M. J.; Char, K.; Lodge, T. P.; Kim, J. K. Transient Solidlike Behavior Near the Cylinder/Disorder Transition in Block Copolymer Solutions. *J. Phys. Chem. B* **2006**, *110*, 15295−15301.
(72) Lu, J.; Bates, F. S.; Lodge, T. P. Addition of Corona Block Homopolymer Retards Chain Exchange in Solutions of Block Copolymer Micelles. *Macromolecules* **2016**, *49*, 1405−1413.
(73) Choi, S.; Bates, F. S.; Lodge, T. P. Molecular Exchange in Ordered Diblock Copolymer Micelles. *Macromolecules* **2011**, *44*, 3594−3604.
(74) Ianniruberto, G.; Marrucci, G. New Interpretation of Shear Thickening in Telechelic Associating Polymers. *Macromolecules* **2015**, *48*, 5439−5449.
(75) Annable, T.; Buscall, R.; Ettelaie, R.; Whittlestone, D. The Rheology of Solutions of Associating Polymers: Comparison of Experimental Behavior with Transient Network Theory. *J. Rheol.* **1993**, *37*, 695−726.
(76) Uneyama, T.; Suzuki, S.; Watanabe, H. Concentration Dependence of Rheological Properties of Telechelic Associative Polymer Solutions. *Phys. Rev. E* **2012**, *86*, 031802.
(77) Liu, C.; He, J.; Ruymbeke, E. v.; Keunings, R.; Bailly, C. Evaluation of Different Methods for the Determination of the Plateau Modulus and the Entanglement Molecular Weight. *Polymer* **2006**, *47*, 4461−4479.
(78) Rubinstein, M.; Semenov, A. N. Dynamics of Entangled Solutions of Associating Polymers. *Macromolecules* **2001**, *34*, 1058−1068.
(79) Fetters, L. J.; Lohse, D. J.; Richter, D.; Witten, T. A.; Zirkel, A. Connection between Polymer Molecular Weight, Density, Chain Dimensions, and Melt Viscoelastic Properties. *Macromolecules* **1994**, *27*, 4639−4647.
(80) Lynd, N. A.; Fredrickson, G. H.; Hawker, C. J.; Kramer, E. J.; Barteau, K. Polymer Electrolytes based on poly (glycidyl ether)s, US8911639B2, December 16, 2014.
(81) Yokoyama, H.; Kramer, E. J. Self-Diffusion of Asymmetric Diblock Copolymers with a Spherical Domain Structure. *Macromolecules* **1998**, *31*, 7871−7876.
(82) Nagarajan, R.; Ganesh, K. Comparison of Solubilization of Hydrocarbons in (PEO−PPO) Diblock Versus (PEO−PPO−PEO) Triblock Copolymer Micelles. *J. Colloid Interface Sci.* **1996**, *184*, 489−499.
(83) Lettow, J. S.; Lancaster, T. M.; Glinka, C. J.; Ying, J. Y. Small-Angle Neutron Scattering and Theoretical Investigation of Poly-(Ethylene Oxide)-Poly(Propylene Oxide)-Poly(Ethylene Oxide) Stabilized Oil-in-Water Microemulsions. *Langmuir* **2005**, *21*, 5738−5746.
(84) Song, J.; Palanikumar, L.; Choi, Y.; Kim, I.; Heo, T.; Ahn, E.; Choi, S.; Lee, E.; Shibasaki, Y.; Ryu, J.; Kim, B. The Power of the Ring: A pH-Responsive Hydrophobic Epoxide Monomer for Superior Micelle Stability. *Polym. Chem.* **2017**, *8*, 7119−7132.
(85) Ma, Y.; Lodge, T. P. Chain Exchange Kinetics in Diblock Copolymer Micelles in Ionic Liquids: The Role of X. *Macromolecules* **2016**, *49*, 9542−9552.

https://dx.doi.org/10.1021/acs.macromol.0c01939
Macromolecules XXXX, XXX, XXX−XXX